# Effects of Soft Encapsulation on the Receive Performance of PMUTs for Implantable Devices

Andrada I. Velea, *Graduate Student Member, IEEE*, Raphael Panskus, Benedikt Szabo, *Graduate Student Member, IEEE*, Vera A. -L. Oppelt, *Graduate Student Member, IEEE*, Lukas Holzapfel, Cyril B. Karuthedath, Abhilash T. Sebastian, Thomas Stieglitz, *Fellow, IEEE*, Alessandro S. Savoia, *Member, IEEE*, and Vasiliki Giagka, *Senior Member, IEEE*

Abstract—**Ultrasound (US) is a promising modality for wirelessly powering implantable devices, requiring encapsulated receivers to ensure long-term stability. Traditional hermetic packaging often limits acoustic transmission, making polymer-based encapsulation a more suitable alternative. This study investigates how implant-grade polymers, thermoplastic polyurethane, parylene-C, and medical-grade silicones (MED-1000, MED2-4213), affect the receive performance of piezoelectric micromachined ultrasonic transducers (PMUTs). Simulations and measurements between 1 and 7 MHz show that all tested materials exhibit transmission coefficients above 94 % at nm- and µm-scale thicknesses, confirming their acoustic transparency. The results show that although coated PMUTs are acoustically well matched with the surrounding water medium, the added mechanical load of the coating can hinder membrane motion and reduce the energy transferred to the PMUTs. Modeling and experimental data demonstrate that stiffer coatings, such as parylene-C, lead to a reduced sensitivity when similar thicknesses are used. Likewise, residual stress in materials like MED-1000 can also degrade performance. These effects are not evident from acoustic transmission measurements alone, underscoring the need to assess both acoustic and mechanical properties when selecting encapsulation materials. In general, softer materials offer excellent acoustic performance for PMUT encapsulation, while stiffer materials must be applied in thinner layers to avoid impairing PMUT function.**

Index Terms—**PMUT, receive performance, soft encapsulation, acoustic characterisation**
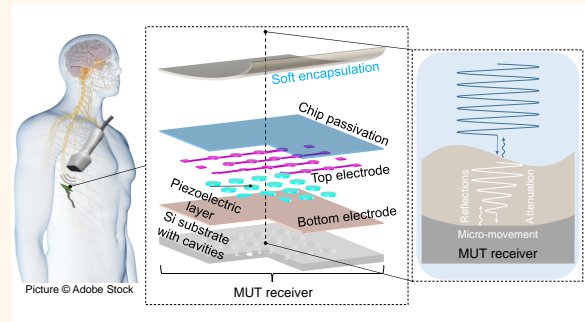
Andrada I. Velea, Raphael Panskus and Vasiliki Giagka are with the Department of Microelectronics, Delft University of Technology, 2628 CD Delft, The Netherlands and with the Fraunhofer Institute for Reliability and Microintegration IZM, 13355 Berlin, Germany (e-mails: a.velea-1@tudelft.nl, r.panskus@tudelft.nl, v.giagka@tudelft.nl).

Benedikt Szabo is with the Department of Microsystems Engineering IMTEK, University of Freiburg, D-79110 Freiburg, Germany and with BrainLinks-BrainTools/IMBIT, University of Freiburg, D-79110 Freiburg, Germany (e-mail: benedikt.szabo@imtek.uni-freiburg.de).

Vera A. -L. Oppelt is with the Department of Microsystems Engineering IMTEK, University of Freiburg, D-79110 Freiburg, Germany and with CorTec GmbH, D-79108 Freiburg, Germany (e-mail: vera.oppelt@cortec-neuro.com).

Lukas Holzapfel is with the Fraunhofer Institute for Reliability and Microintegration IZM, 13355 Berlin, Germany (e-mail: lukas.holzapfel@izm.fraunhofer.de).

Cyril B. Karuthedath and Abhilash T. Sebastian are with the VTT Technical Research Centre of Finland Ltd, Espoo, Finland (e-mails: cyril.karuthedath@vtt.fi, abhilash.thanniyil@vtt.fi).

Thomas Stieglitz is with the Department of Microsystems Engineering IMTEK, University of Freiburg, D-79110 Freiburg, Germany, with BrainLinks-BrainTools/IMBIT, University of Freiburg, D-79110 Freiburg, Germany and with Bernstein Center Freiburg, University of Freiburg, D-79110-Freiburg, Germany (e-mail: thomas.stieglitz@imtek.uni-freiburg.de).

Alessandro S. Savoia is with the Department of Industrial, Electronic, and Mechanical Engineering, Roma Tre University, 00146 Rome, Italy (e-mail: alessandro.savoia@uniroma3.it).

I. INTRODUCTION

ADVANCES in the field of implantable devices focus on miniaturization, wireless powering, efficient energy transfer, and highly specific neuromodulation. For wirelessly powered implants, ultrasound (US) has emerged as a promising candidate, particularly for deep-seated implants, due to its efficient propagation through biological tissue. Research shows that US is able to communicate with [1] and deliver high power levels to millimeter-sized (mm-sized) implants at depths over $10\,\mathrm{cm}$ inside the human body [2], [3], making it a promising alternative to radio frequency (RF) and inductive coupling methods [4]. Another important advantage is the high ($720\,\mathrm{mW\,cm^{-2}}$) FDA-approved limit for the spatial-peak temporal average acoustic intensity (I_{SPTA}) [5]. Using US for powering requires at least two transducers: a transmitter (TX) and an implant-integrated receiver (RX). To enable further miniaturization, micromachined US transducers (MUTs) are currently being investigated. For implantable devices, packag-

Highlights

- **We analyze how polymers used as implantable device coatings impact PMUT receive performance, considering their acoustic properties, mechanical effects, and acoustic mismatches.**
- **Simulations and measurements show that polymers up to µm thicknesses have a transmission coefficient above 94 %, but residual stress or higher stiffness can reduce the receive sensitivity of encapsulated PMUTs.**
- **Ultrasound is a promising candidate for powering deep-seated implants and polymer encapsulation can, upon careful consideration of the acoustic, mechanical properties and thicknesses, have minimal impact on PMUT performance.**

ing is crucial, and conventionally, hermetic (either metal or ceramic) cases are being used [6]. However, US transducers require an acoustically conductive medium for optimal sound wave propagation. Metal or ceramic cases (filled with dry gas) hinder signal transmission due to their higher characteristic acoustic impedance, compared to water or biological tissue, causing strong reflections. In an attempt to overcome this, ceramic packages, filled with polydimethylsiloxane (PDMS), and with thin metal lids have been proposed for PZTs to enable ultrasonic coupling while preserving hermeticity [7]. However, the assembly process is cumbersome, and both ceramics, and thin metal layers are prone to cracking, leading to failure and a decreased lifetime of devices. More recent studies [8] and [9] have explored the use of conformal coatings for implantable devices, demonstrating stability even after in-vivo implantation. Within this frame, investigating similar polymers for the encapsulation of transducers is, therefore, essential. For MUTs in particular, not only do the bulk properties of the encapsulation materials directly influence longitudinal wave propagation, but shear properties and viscoelasticity also play a critical role on the transducer flexural vibration [10]. Hybrid hermetic-soft approaches were proposed for capacitive MUTs (CMUTs) in implant applications, where a soft material couples the transducer to the hermetic package [11]. However, this method can still cause unwanted multiple reflections between the soft and hard layers, leading to additional loss, and thus, a polymer-based encapsulation is a more promising approach for ultrasonically powered implants. However, variations in material properties, thicknesses, and deposition methods, can affect the received signal on the RX transducer. This paper systematically analyzes how different polymers affect the receive performance of PMUTs by considering the acoustic properties of the materials, their mechanical influence and acoustic mismatches between the soft polymer layers and the harder PMUT layers.

The paper outlines the PMUT structure, encapsulation processes, and simulation/ experimental methods in II. Methods. It compares materials and devices with simulations, presents the measurement setup and sample characterisation results in (III. Results and Discussion), and concludes the study in IV. Conclusion.

II. METHODS

A. Piezoelectric Micromachined Ultrasonic Transducers (PMUTs)

2x2 cm^2 arrays of PMUTs built on Cavity Silicon on Insulator (C-SOI) wafers (Okmetic, Vantaa, Finland), were
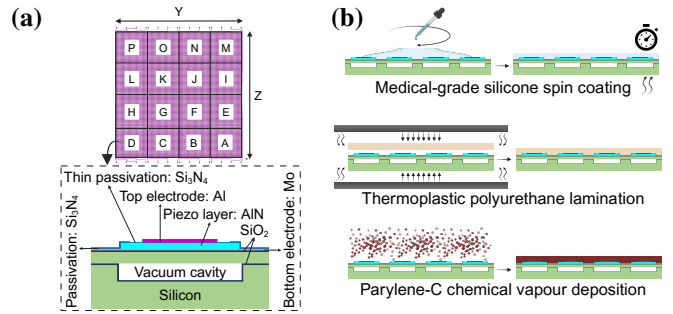

Fig. 1 Test structures and encapsulation methods (*Created with BioRender.com*). **(a)** Top-view of the PMUT array layout including distribution of the 16 elements and a cross-section schematic representation of one PMUT cell. **(b)** Description of the encapsulation processes used (i.e., spin coating for medical-grade silicones, lamination for thermoplastic polyurethane, and chemical vapour deposition for parylene-C).

used. Each device comprises 20 736 cells, each with a diameter of 70 µm and spaced at a 120 µm pitch. The cells are grouped in 16 independently addressable elements (5x5 mm^2), labeled from A to P, each comprising 1296 cells (**Fig. 1(a)**). The basic structure of a PMUT cell, shown in **Fig. 1(a)**, consists of a C-SOI substrate with a silicon dioxide (SiO_2) passivation layer. The vibrating element (i.e., aluminium nitride (AlN) layer) is sandwiched between a bottom molybdenum (Mo) and a top aluminium (Al) electrode. Finally, a silicon nitride (Si_3N_4) layer acts as passivation for the entire array [3]. The PMUTs have a resonance between 4.5–4.7 MHz in air, and ~ 2.9 MHz in water, with a significantly larger bandwidth.

B. Encapsulation materials and processes

The polymers listed in **Table I** were used for the material investigations. Epoxy resins, a distinct category, have high strength and good adhesion. However, these were excluded from the study as they are generally very stiff compared to other soft materials [12], and brittle as a result of their highly cross-linked thermoset structure. This can lead to cracking under stress, thermal cycling, mechanical loads, or in body environments, especially in thin layers [8], [13]. Upon preliminary theoretical and experimental analysis of the individual materials, for the encapsulation of PMUTs, the material choice has been limited to Platilon 4201 AU thermoplastic polyurethane (TPU), parylene-C, MED-1000, and MED2-4213 silicones. The encapsulation procedure for TPU, consisted in laminating 25 µm thick material sheets using a cleanroom-

TABLE I Material classes and specific types used in the study

Material Class	Material Name	Type	Supplier
Polyurethane	Platilon 4201 AU	Thermoplastic polyurethane (TPU)	Covestro AG, Germany
	Bionate II 80A	Medical-grade thermoplastic polycarbonate polyurethane (PCU)	DSM-Firmenich, The Netherlands
Silicone	MED2-4213	Medical-grade two-component	NuSil Technology LLC, USA
	MED-1000	Medical-grade one-component	NuSil Technology LLC, USA
Parylene	parylene-C	type C	Galentis S.r.l., Italy
Polyimide	LTC9320		Fujifilm, Belgium

compatible thermocompression process at 6–7 bar and 160 °C. Due to the thermoplastic nature of the material and the low topography of the PMUTs, the TPU lamination process has the potential of providing reliable tens of µm-thick conformal coatings. The used temperature and pressure does not affect the structural integrity of PMUTs [14]. For parylene-C, 5 µm were deposited by means of chemical vapour deposition (CVD), where parylene monomers were deposited onto the surface of interest at 30 °C and 25 µbar. The CVD process offers high conformal coatings even when a few µm-thick layers are desired. For silicones, a spin-coating process was employed. First, both MED-1000 and MED2-4213 were diluted with 50 % n-Heptane and spin-coated at a rate of 1000 rpm. MED-1000 cured at room temperature in approximately 72 hours, while MED2-4213 was cured at 150 °C for 15 min under 1.8 bar. No primer was used during the spin-coating process. Even if the topography of the PMUTs is not significant, a spin-coating process may still lead to non-uniformity (particularly thickness variation between center and edges) or potential defects of the layers (presence of gaps between the PMUT and the coating, caused by lower adhesion, particularly when no primers are used, or shrinkage, and temperature cycling are significant).

C. Acoustic characterisation of coatings

We analysed the acoustic properties of the selected coating films by simulating and measuring the acoustic wave transmission coefficient (T) through polymer layers of varying thickness. For the simulations, we selected three thicknesses (100 nm, 25 µm, and 1 mm), covering a wide range from nm to mm scale. These correspond to the main deposition techniques (CVD, spin-coating, and lamination) used to encapsulate PMUTs. The 100 nm layer could also minimize mass loading, thus preserving the resonance frequency and sensitivity of PMUTs. Despite the water vapour permeability of polymers, good adhesion and uniform interfaces can ensure long-term stability, making thin layers viable encapsulants ([8], [9]). For the experiments, different thicknesses were used depending on the setup. In the transmission measurements through free-standing films, thicknesses of 25 µm Platilon TPU, 12 µm Bionate PCU, 100 µm MED2-4213, 35 µm MED-1000, 22 µm parylene-C, and 20 µm polyimide were chosen for mechanical stability and ease of handling. In the PMUT-based measurements (impedance and receive sensitivity), application-relevant coatings: 25 µm Platilon TPU, 37 µm MED2-4213, 45 µm MED-1000, and thinner, such as 5 µm parylene-C, were used to reflect practical use and avoid affecting cell performance. All thicknesses were chosen based
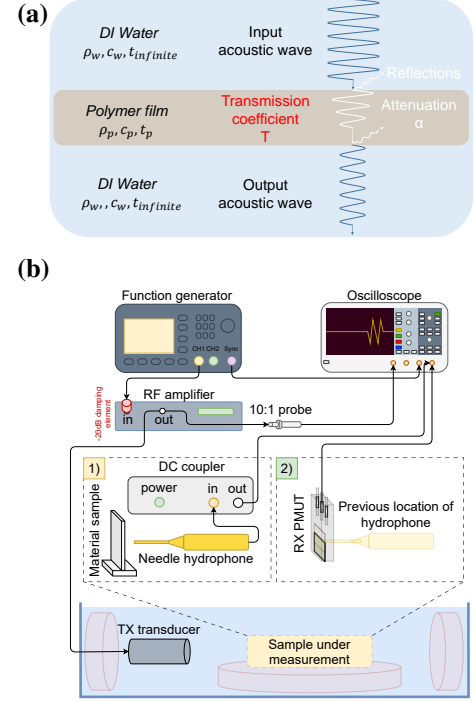

Fig. 2 Simulation model and test setup used for evaluating the transmission coefficient. **(a)** Simulation model for the polymer film materials, where ρ represents the density, c, the speed of sound, t, the thickness, α, the attenuation, and T the simulated and measured transmission coefficient. **(b)** Experimental setup used for measuring the transmission coefficient through polymers (measurement 1, in yellow) as well as the open circuit voltage (OCV) of coated and uncoated PMUTs (measurement 2, in green) (*Created with draw.io*).

on deposition methods and compatibility with microfabricated topographies. Numerical simulations based on [15], and described in detail in [16] assume continuous transmission of planar waves, with pressure and particle velocity continuity at each boundary. As illustrated in **Fig. 2(a)**, the model estimates T through various material films, in a semi-infinite water medium, taking into account reflections and attenuation of the acoustic wave. The material properties used in the simulations are listed in **Table II**. Density, ρ, speed of sound, c, acoustic impedance Z (the product of density and speed of sound), and bulk attenuation, α at 5 MHz were measured according to the methodology described in [17] using 40x40x2 mm^3 material slabs. The thickness was chosen such that the material samples were significantly thicker than the wavelength, and

thus the parameters of interest were accurately extracted. Since for parylene-C and polyimide, such thicknesses were unachievable, the values were based on previous literature. Attenuation is a property dependent on and proportional to the frequency used and the thickness of the material. Although TPU, has high attenuation at 5MHz, at the target thickness ($25\,\mu$m), attenuation and related losses are low ($\sim 0.1\,$dB). Therefore, if compared to an average attenuation for soft tissue (~ 0.5–$0.7\,$dB cm^{-1} MHz^{-1} [18], [19]), particularly if an implant comprising encapsulated PMUTs is placed deep inside the body, such attenuation of the encapsulation layer will have a minimal impact. For the measurements, material films were placed inside a water tank, between an unfocused $5\,$MHz transmit (TX) transducer (V309-SU, Olympus, Tokyo Japan) and a $1\,$mm needle hydrophone (NH1000, Precision Acoustics, Dorchester, UK) (**Fig. 2(b)**, measurement 1, in yellow). The TX transducer was driven using $20\,\mu$s sinusoidal bursts, modulated by a Hann window, thus resulting in a variable number of cycles per frequency, generated by a function generator (Keysight 33600A, California, USA). The pulse width was $20\,\mu$s with $4\,\mu$s rising and falling edges, a pulse repetition frequency (PRF) of $20\,$Hz and the peak-to-peak amplitude of $1\,$V. The signal was amplified using an RF amplifier (350L, E&I, New York, USA) with a $47\,$dB nominal gain. First, reference measurements (without a polymer film) were taken, for frequencies between $1\,$MHz and $7\,$MHz, in steps of $1\,$MHz which include the resonant frequencies of the PMUTs, both in air and in water, at a distance of $10\,$cm. To record the acoustic pressure through materials and convert it into an electrical signal, the needle hydrophone was connected through a DC coupler (Precision Acoustics, Dorchester, UK) to an oscilloscope (RTA4004, Rhode&Schwarz, Munich, Germany). On the walls of the water tank, particularly behind the hydrophone, under the sample, and lateral to the transducer, sample, and hydrophone, absorbers (VK-76000, Gampt, Merseburg, Germany) were placed in order to reduce reflections from the tank walls. To further minimize errors and maintain consistent measurement conditions, the samples were positioned using a motorised 3D stage (SFS630, Gampt, Merseburg, Germany) at an equal $10\,$cm distance both from the transducer and the hydrophone. This minimizes reflections, preventing interference with the measured signal. To verify this, a $7\,$MHz single-cycle pulse was sent through the polymer and the time delay between the first reflection and the main recorded signal was monitored. The hydrophone-transducer distance was adjusted to ensure a time delay over $20\,\mu$s, which is the pulse width used during the experiments. Pressure through the polymer samples was then measured and the transmission coefficient was calculated by subtracting the material measurements from the reference measurements (assumed to have a normalized transmission coefficient of 1), at each frequency.

D. Acoustic characterisation of encapsulated PMUTs

1) Finite Element Modelling (FEM): Finite element modeling (FEM) using ANSYS (Ansys Inc., Canonsburg, PA, USA) was performed to predict the behavior of coated and uncoated

TABLE II Material properties used for simulations

Material Name	Density [ρ] kg/m^3	Speed of Sound [c] m s^{-1}	Acoustic Impedance [Z] MRayl	Attenuation at $5\,$MHz [α] dB mm^{-1}
TPU Platilon 4201AU	1150	1750	2.012	5.08
PCU Bionate II 80A	1200	1833	2.199	6.24
Silicone MED2-4213	1110	1125	1.248	1.55
Silicone MED-1000	1080	1000	1.08	2
Parylene-C [20]	1289	2135	2.752	1.5
Polyimide LTC9320 [21]	1419	2142	3.039	2.91
Water	1000	1480	1.48	0.055

PMUTs in terms of electrical impedance and receive sensitivity. A 3D FEM model of a periodic layout of circular PMUT cells arranged in a square grid pattern, with the layer stack described in II-A, was implemented using ANSYS APDL. The top of the cells is encapsulated, while the $660\,\mu$m-thick bulk Si of the PMUT is in contact with a $1.55\,$mm-thick FR4 printed circuit board (PCB). Both the PMUT cells and the FR4 layer are coupled to a fluid medium (water). The solid and fluid materials were meshed using hexahedral SOLID185 and FLUID30 elements, respectively, while SOLID226 elements were used to model the piezoelectric transduction effect. To approximate coupling to an infinite propagation medium, total reflection was assumed at the boundaries of the top and bottom fluid domains. The acoustic attenuation in the encapsulation layer was modeled using a linear viscoelastic model, employing a Prony series representation of bulk relaxation behavior. The coefficients of the Prony series were fitted to match the experimentally estimated bulk attenuation around $5\,$MHz, following established methods for frequency-dependent damping in soft polymers [10], [22]. To calculate the electrical impedance, a voltage generator modeled using the CIRCU94 element was applied to the top and bottom electrodes of the PMUT cells. Harmonic analyses were performed with a uniform voltage excitation over the 1–$7\,$MHz range for the bare PMUT in air and water, as well as for different encapsulation materials under water-coupled conditions. To calculate the receive response, a uniform pressure excitation was applied at the center of the fluid domain to generate a plane wave directed towards the PMUT. Harmonic analyses were then conducted over the same frequency range for each encapsulation material in water-coupled conditions. Platilon TPU ($25\,\mu$m), parylene-C ($5\,\mu$m), MED-1000 ($45\,\mu$m) and MED2-4213 ($37\,\mu$m) silicones were considered for FEM modelling, as these were later used for PMUT encapsulation and analysis. The acoustic and mechanical properties used in the simulations have been presented in tables II and III. Additionally, preliminary COMSOL modelling has been employed to simulate the forces at the interfaces between MED-1000 silicone and the PMUT cells. The model uses a $7.43\,\mu$m size triangular mesh, and it assumes PMUT cells with the layer stack described in II-A and a $100\,\mu$m encapsulation layer on top.

2) Impedance measurements: Impedance on uncoated and coated PMUTs was measured with 1601 points per measurement, between $1\,$MHz and $7\,$MHz using an impedance analyzer (Keysight E4990A, California, USA). A total of 144 individual elements from nine uncoated and wire bonded samples were measured in air and deionized (DI) water (an excellent coupling medium with acoustic impedance similar to

soft tissue). For the water-coupled measurements, each PMUT sample was placed inside the water tank, facing an absorber to prevent reflections from influencing the measurements. Next, the samples were coated with different polymers, as described in II-B, and remeasured. Each polymer was deposited on a separate uncoated sample (a total of 16 elements per polymer were measured). Encapsulation with Platilon TPU was not possible on wire-bonded PMUTs due to potential damage of the wires during the encapsulation process. Thus, the sample was first coated, then wire bonded and its impedance measurements were compared to other uncoated devices. Since PMUTs show broadband behavior in DI water, air-coupled impedance measurements were primarily used for comparison. An initial system calibration was required, considering additional components, such as cables and PCB, thus increasing the signal-to-noise ratio. For the uncoated devices, measurements were first averaged across elements within each device. The final plotted result represents the average of these element-averaged values across all uncoated samples, along with the standard deviation. For the coated devices, since each coating corresponds to a single device, measurements were averaged across elements, and this average was plotted with its associated standard deviation.

3) Receive sensitivity measurements of PMUTs: Measurements on uncoated and coated PMUTs were conducted to evaluate the effect of soft encapsulation on the received energy. The setup in **Fig. 2(b)** (measurement 2, in green) is the same as for the material characterization, but the material samples were replaced by functional PMUTs. First, the output pressure of the TX transducer (described in II-C) was evaluated in its far field, at a fixed axial distance of $25\,\mathrm{cm}$, corresponding to the position where the PMUT was later placed for evaluation. Manual alignment was employed to determine the lateral position of the hydrophone with respect to the TX transducer, where the maximum output pressure of the transmitter was recorded. At that fixed location, the output pressure was then measured over frequencies between $1\,\mathrm{MHz}$ and $7\,\mathrm{MHz}$, in steps of $0.2\,\mathrm{MHz}$. The input impedance of the oscilloscope was set to $1\,\mathrm{M\Omega}$. Additionally, a second 2D scan measurement was performed to further evaluate any changes in the beam profile of the TX transducer, over the frequencies of interest. Finally, the recorded voltage (for both types of measurements) was converted into pressure, considering the sensitivity of the needle hydrophone used (**Fig. 5(c)**). To measure individual elements, the PMUT was moved in the Y and Z directions with respect to the TX transducer, using an automated 3D stage. The measured open circuit voltage (OCV) of each PMUT element was recorded, once, for each frequency. Given the measured OCV and the pressure at the PMUT location, the RX sensitivity of each element was calculated by dividing the two values, and the average over all elements, and the respective standard deviation were plotted. Since more uncoated devices were measured, the averaging and standard deviation were calculated and plotted following the same principle described in II-D.2. Small variations in the measurement setup, such as water level and sample positioning, could introduce errors. To address these, the setup was further characterized, by evaluating lateral and angular misalignments between the TX

transmitter and PMUTs. The TX transducer was first aligned with respect to the PMUT, driven as described in II-C, in steps of $1\,\mathrm{MHz}$ and moved with respect to the PMUT as follows: for the lateral misalignment measurements, in steps of -$1\,\mathrm{mm}$ and $1\,\mathrm{mm}$ in Y and Z, and for the angular misalignment, in steps of $1°$, left and right. The measurement error was either evaluated across 10 consecutive measurements, with the error calculated and plotted as a standard deviation, or by changing the measurement conditions after each measurement.

III. RESULTS AND DISCUSSION

A. Acoustic characterisation of coatings

The selected thickness range for evaluating the transmission coefficient reflects typical values for neural interface substrates and encapsulation. **Fig. 3(a)** highlights key dependencies for the frequency range of interest: material attenuation differences at the same thickness and distinct resonance peaks in thicker films due to changing resonance conditions. A preliminary classification for the materials can be derived with MED2-4213, overall having the highest transmission coefficient due to the relatively low attenuation and minimal acoustic impedance mismatch with water (**Table II**). It is followed by parylene-C, MED-1000 (although this can alternate for low frequencies and thin layers, it can be assumed that the difference between the two materials is relatively small), polyimide, and polyurethane (Platilon and Bionate). For thicknesses in the nm-range, the transmission coefficient remains above 99.9%, with negligible losses. Even for μm-range, although T has a tendency to drop for some materials, T is always above 90% at a maximum frequency of $7\,\mathrm{MHz}$. As shown in **Fig. 3(b)**, the measured (solid lines) and simulated (dashed lines) transmission coefficients align. The thicknesses for the material samples were different and dependent on the deposition processes. The larger variations observed for silicones are likely due to the non-uniformity of the spin-coated layers. This was most notable for MED2-4213, where white light interferometry showed μm-scale surface roughness. Yet, T remained above 94% in all cases.

B. Mechanical analysis of coatings

Mechanical properties and residual stress inside polymers may limit the movement of PMUT cells, potentially reducing their performance. The two silicones investigated have different crosslinking mechanisms: MED-1000, a one-component self-curing silicone, cures in the surrounding humid atmosphere, but exhibits a shrinkage effect, potentially affecting membrane deflection. MED2-4213, a two-component silicone, cures without shrinkage and thus without internal stresses. Preliminary COMSOL modelling shows that the residual stresses of MED-1000 silicone layer are $4\,\mathrm{kPa}$, leading to an upward lift of the membranes of approximately $4\,\mathrm{nm}$. To support the future selection of materials and thicknesses for PMUT encapsulation, the tensile strength, Young's modulus as well as elongation properties (**Table III**), were analysed, from a theoretical perspective. For example, polyimide is significantly stiffer, with a Young's modulus 3–4 orders of magnitude higher than silicones and TPU, and elongation one order of magnitude
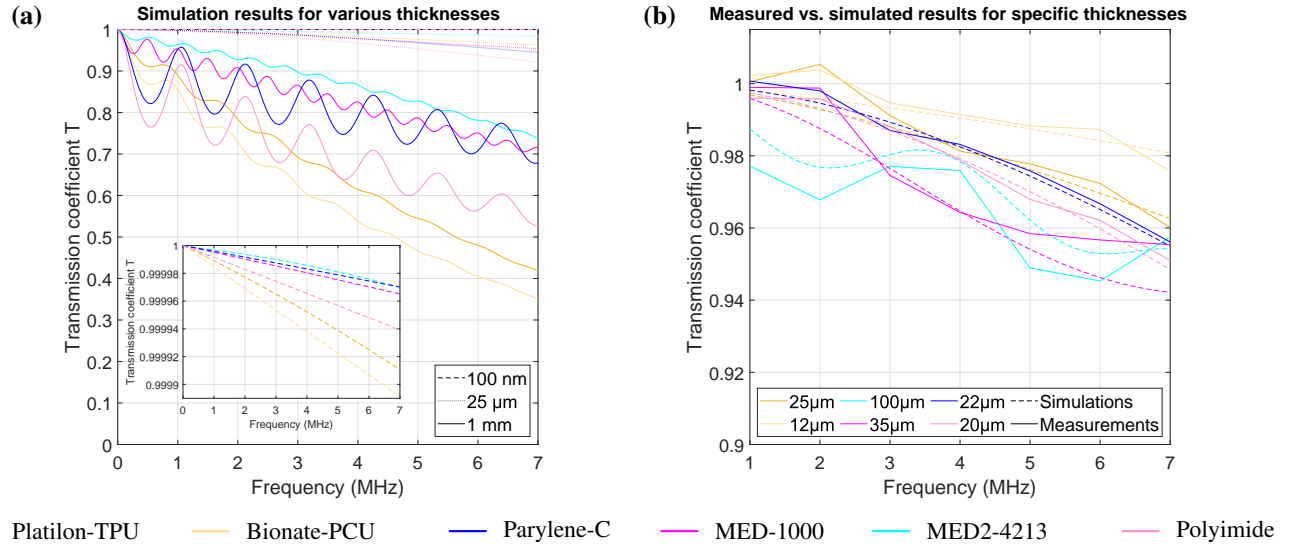
Fig. 3 Acoustic characterisation of materials. **(a)** Simulated transmission coefficient through polymer thicknesses of $100\,\text{nm}$, $25\,\mu\text{m}$, and $1\,\text{mm}$. An inset for thin layers ($100\,\text{nm}$) was added. The transmission coefficient decreases with increasing thicknesses and frequencies. The resonance peaks and changes in resonance conditions are visible, particularly for thick layers. **(b)** Measured (solid lines) transmission coefficient juxtaposed against simulations (dashed lines) for thicknesses and materials of choice. The transmission coefficient in all considered cases is above $94\,\%$.

lower than the rest of the materials. Since it is expected to restrict the movement of the PMUT cells, thus significantly reduce the receive sensitivity of the devices, it was excluded from further studies in this paper.

C. Electrical impedance analysis

Air- and water-coupled electrical impedance was evaluated by means of FEM and measurements on coated and uncoated PMUT samples, and the results are shown in **Fig. 4**. The air-coupled simulations in **Fig. 4(a)** indicate a shift in the resonance peaks for the encapsulated PMUTs, from $\sim 4.7\,\text{MHz}$ to frequencies between $2.1\,\text{MHz}$ and $2.5\,\text{MHz}$ for silicone and TPU-coated PMUTs, and $\sim 4.2\,\text{MHz}$ for parylene-C-coated PMUTs. This is due to the fact that the additional layers change the resonator characteristics of the PMUT by adding additional mass and stiffness to the membranes. A stiffer coating, such as parylene-C, often indicates a higher resonance frequency, compared to softer polymers, such as silicones and TPU (**Fig. 4(a)**). The dampened peaks can be attributed to the viscoelasticity of the polymers, which in turn can lead to energy dissipation within the coating. The slightly wider resonance peaks (for TPU and parylene-C-coated samples) indicate an improvement in the acoustic matching by providing a better transition between the high PMUT and the low air

TABLE III List of mechanical properties of chosen polymer families

Material Name	Tensile Strength MPa	Young's Modulus MPa	Elongation %
Polyurethane [23]	24.8 ± 1.7	33.4 ± 3.0	Up to 336
Silicone [24]	6.2	0.3 ± 0.2	Up to 600
Parylene-C [25], [26]	55.16	2750 - 4500	Up to 200
Polyimide [24]	392	8830	Up to 30

acoustic impedance. A similar effect occurs when the samples are water-coupled. As shown in **Fig. 4(b)**, the resonance peaks are significantly broadened in water, for all PMUTs, regardless of their coating. The inset reveals this broad resonance, centered around $3\,\text{MHz}$. This in turn, indicates a significant improvement in the impedance matching between PMUTs and the surrounding medium. Although some variations are present, the measured results in **Fig. 4(a)**, and **Fig. 4(b)** (air- and water-coupled) show similarities to the simulations. The measured air-coupled resonance frequency in **Fig. 4(a)**, for the $45\,\mu\text{m}$ thick MED-1000 silicone and $25\,\mu\text{m}$ TPU-coated devices, shifts to lower values, as predicted by the simulations. In **Fig. 4(a)**, it can be noted that the resonance peak for the $5\,\mu\text{m}$ parylene-C-coated devices is highly damped and widened, possibly due to internal stresses in the film which modify the overall stiffness of the membrane, introducing additional damping. An interesting discrepancy arises in the $37\,\mu\text{m}$ MED2-4213-coated samples, where the measured air-coupled resonance frequency is higher than in simulations (**Fig. 4(a)**). A likely cause can be the partial detachment of the material from the surface of the PMUT, leading to the presence of gaps between the PMUT and the encapsulation (i.e. air interface), which could lead to an increase in the resonance frequency. These types of defects could be assessed using destructive techniques such as cross-sectioning or focused ion beam-scanning electron microscopy (FIB-SEM). However, since these methods cause irreversible damage to the samples, they were not used. It can also be noted that the standard deviation in the phase plot increases with frequency, both for the air- and water-coupled measurements (**Fig. 4(a)** and **Fig. 4(b)**). This is most likely a systematic effect due to a non-perfect system calibration prior to the measurements. Although the scale for the plots in these figures is different
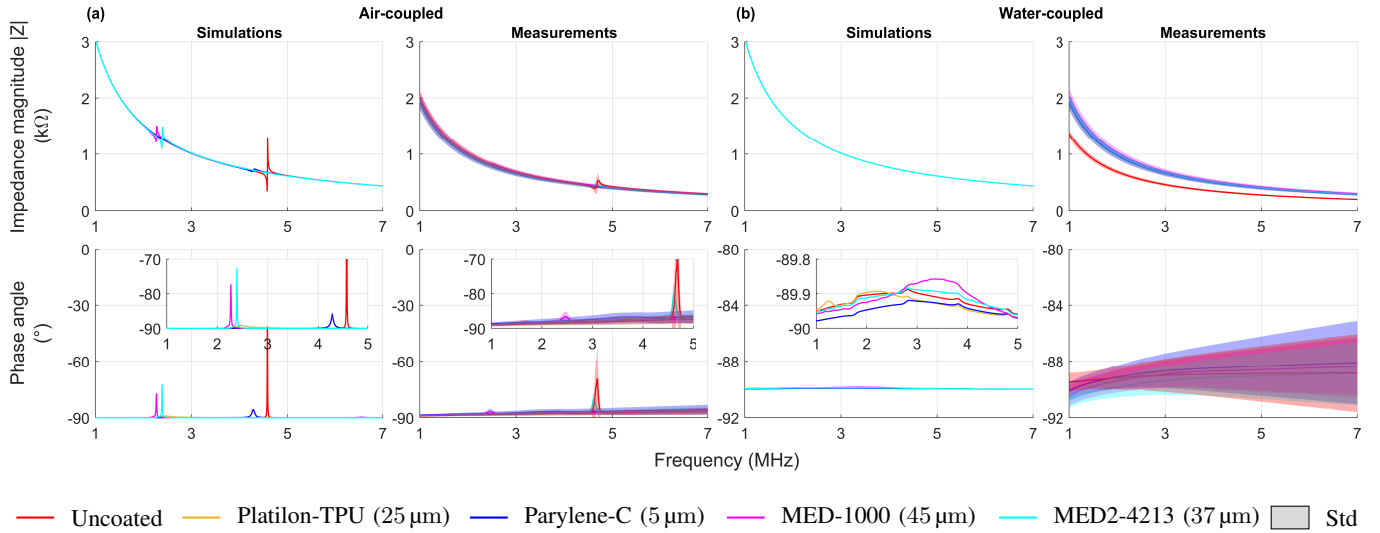
Fig. 4 Impedance evaluation of coated and uncoated PMUTs. **(a)** FEM simulations and measurements of air-coupled electrical impedance. The resonance peaks, together with the frequency shift and dampened peaks for the simulated encapsulated samples can be observed. Measurements show higher resonance for MED2-4213-coated samples than simulations, potentially due to the presence of air gaps between the encapsulation and the PMUTs. **(b)** FEM simulations and measurements of water-coupled electrical impedance. The broadband behavior of the PMUTs in DI water makes the resonance peaks not clearly visible. The large standard deviation in the phase can be attributed to the on-chip resistance of the PMUTs.

for a better illustration of the results, the standard deviation trend is similar. During calibration, the additional components comprising the setup are taken into account, except for the on-chip resistance of the PMUT, which is larger for inner elements, due to the longer traces to the pads. This, in turn, adds to the overall electrical impedance. The water-coupled simulations in **Fig. 4(b)** assume the real-case scenario, where the PMUT was stacked on top of a PCB and surrounded by water. The variations observed in the measured phase plot, compared to the simulations can be caused by the on-chip resistance of the PMUTs. Although a correction was applied by subtracting the on-chip resistance (assumed to be the real part of the air-coupled impedance at high frequencies) from the water-coupled measurements, the correction factor may still vary more than estimated.

D. Receive sensitivity of uncoated and coated PMUTs

The simulated results, illustrated in **Fig. 5(a)**, show that for all coated PMUT devices, the receive sensitivity is comparable to that of an uncoated PMUT. Small deviations are present, particularly for the parylene-C-coated sample, where a maximum drop in RX sensitivity of $\sim 25\,\%$, at low frequencies can be observed. This drop in the receive sensitivity is also observed in **Fig. 5(b)** and can be attributed to the mechanical properties of the material (i.e., stiffness) rather than to the acoustic ones. As shown in **Fig. 3**, all materials with thicknesses of tens of µm, exhibited T above $94\,\%$ across the 1–$7\,\text{MHz}$ range. Therefore, the selected materials and coating thicknesses can be considered acoustically transparent. Although parylene-C is intrinsically stiffer than the other polymers, reflected in its higher Young's modulus (**Table III**), a property independent of thickness, the mechanical loading it introduces depends on its flexural rigidity, which is a function

of both Young's modulus and the cube of the thickness. Consequently, using thinner parylene-C layers could reduce mechanical damping of the PMUT membrane and potentially improve receive sensitivity. However, depending on the application, further reduction in thickness may not be feasible due to constraints related to handling, mechanical durability, or encapsulation performance. The simulations shown in **Fig. 5(a)**, as well as the measurements in **Fig. 5(b)** reveal periodic resonance peaks which can be attributed to the PCB material, having the fundamental frequency around $1.5\,\text{MHz}$ and all other harmonics at higher frequencies. Moreover, for the TPU-coated sample, at frequencies around $1\,\text{MHz}$ (**Fig. 5(a)**), an additional peak can be observed. This can be attributed to one of the shear mode resonances of the material itself. These however, do not seem to affect the RX sensitivity of the simulated samples. For the measured samples, however, the frequency at which the peaks appear does not accurately match the simulations. This is due to the mismatch between the assumed PCB material properties and the actual values. The slight decrease in the overall recorded sensitivity magnitude (**Fig. 5(b)**) for all samples, compared to the simulations (**Fig. 5(a)**) is expected and assumed to be caused by additional components such as cables, that are not considered in the simulations, by the error introduced by the measurement setup (**Fig. 6(a)**), or by the low TX sensitivity of the transmitter at the resonance frequency of the PMUTs (**Fig. 5(b)**). If variations occur between samples, this will be reflected in the averaged results. It is important to note that in case some of the elements under measurement were completely unresponsive due to damage to the membranes or to the wire bonds, they have been excluded from the averaging and, thus, from the final analysis. Compared to the simulations, the trend in the measurement results is generally followed by the PMUTs. For
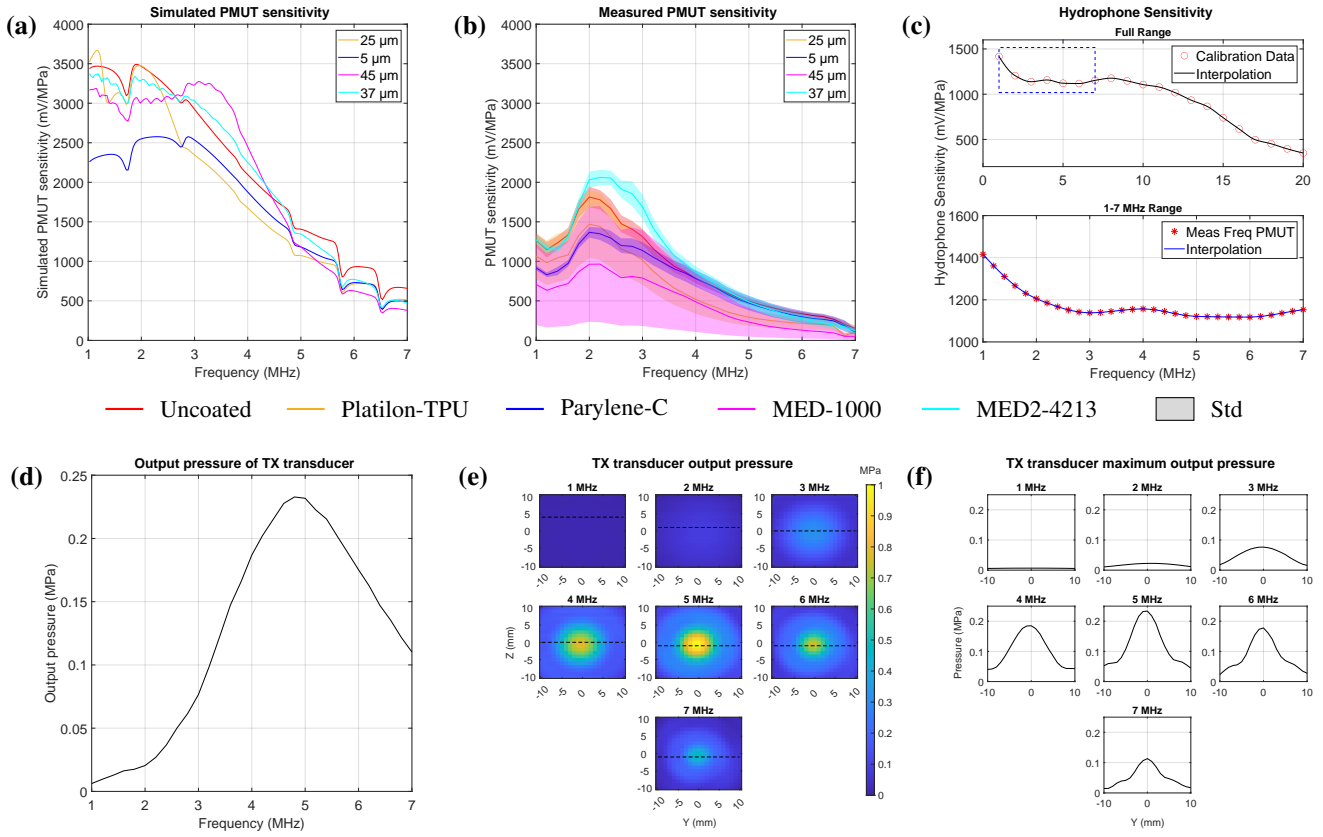
Fig. 5 Receive sensitivity of PMUTs. **(a)** FEM simulations. Coated samples exhibit similar receive sensitivity as uncoated PMUTs. A maximum drop of 25 % in the receive sensitivity at low frequencies can only be observed for a simulated parylene-C-coated sample. **(b)** Receive sensitivity measurements of PMUTs. The measured receive sensitivity of MED-1000 coated PMUTs is significantly lower than predicted in the simulations, potentially due to the residual stress applied by the polymer. **(c)** Sensitivity of a 1mm needle hydrophone, plotted according to the values specified in the datasheet. **(d)** Output pressure of TX transducer measured in its far field, at a distance of 25 cm. The highest output pressure is measured around the resonance frequency of the transducer. **(e)** 2D scan of the output pressure of TX transducer measured in its far field, at a distance of 25 cm. The dotted line represents the area of highest intensity and is then plotted in (f) to illustrate the beam width. **(f)** Width of the TX beam extracted from the 2D scans of the measured output pressure of the TX transducer. The change in output pressure as well as beam profile is visible with the change in frequency.

MED2-4213, it can be observed (**Fig. 5(b)**) that the sample exhibits an RX sensitivity similar to the average RX sensitivity of uncoated PMUTs, thus accurately matching the simulations. White light interferometry showed that MED2-4213-coated samples had a thickness variation of a few μm from center to the edge. However, due to the fact that its acoustic impedance is closer to water, leading to little reflections at the interface, increased softness, and lack of residual stress upon curing, the thickness variation does not have a negative impact on the overall receive sensitivity. The predicted RX sensitivity for MED-1000, on the other hand is not reproduced by the measurement results. The drop in sensitivity as well as large standard deviation (larger than for the rest of the samples) can be attributed to the residual stresses that the material applies to the PMUT cells, as discussed in III-B, potentially leading to a partial detachment of the material, limiting acoustic wave transmission to the PMUT cells, and thus significantly reducing the measured OCV, which, in turn, results in a decrease in the received pressure. The spin-coated layer, as opposed to MED2-4213, did not indicate a thickness variation.

Similar to MED2-4213, MED-1000 is soft, with an acoustic impedance closer to water. The only differentiating factor, which leads to a significant drop in the receive sensitivity is the shrinkage effect present upon curing. For TPU-coated samples, the measured RX sensitivity is lower than predicted and assumed to be such due to the non-uniformity of the laminated layer. The white light interferometry indicated a surface roughness in the hundreds of nm scale and a thickness variation of a few μm. Although the variation is similar to the one for MED2-4213, this, coupled with the higher acoustic impedance of TPU, resulting in more reflections, as well as its increased stiffness compared to MED2-4213, limiting the free movement of the membrane, leads to a drop in the measured RX sensitivity. Another important aspect observed in the measured data in **Fig. 5(b)** is the decreased RX sensitivity at particular frequencies. This can be caused by the fact that frequencies above $\sim 4\,\mathrm{MHz}$ are outside the frequency bandwidth of the PMUTs, in water. Moreover, frequencies around $1\,\mathrm{MHz}$ are also outside the frequency bandwidth of the TX transmitter (an effect shown in **Fig. 5(d)**). Therefore,
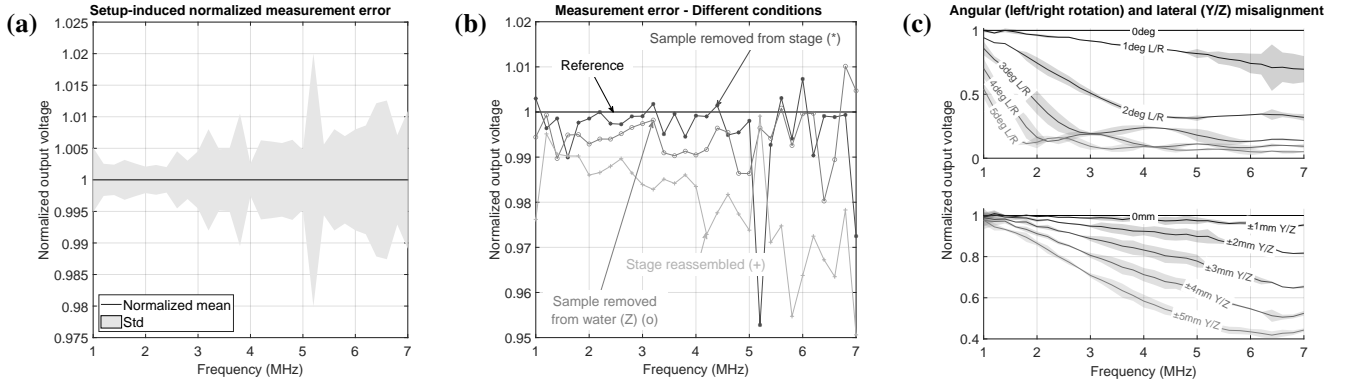
Fig. 6 Measurement variability and setup error. **(a)** Measurement error after 10 consecutive measurements on the same sample. A maximum error of $\pm 2\%$ was recorded, at $5\,\mathrm{MHz}$, whereas a maximum error of $\pm 0.5\%$ was measured at $2.9\,\mathrm{MHz}$, the resonance frequency of the PMUTs. **(b)** Normalized single OCV measurements for one uncoated RX PMUT under different setup conditions. The highest drop is observed when the measurement setup is partly reassembled, between measurements. **(c)** Error from angular misalignments of up to $5°$ in both left (L) and right (R) directions of the TX transducer relative to the measured PMUT. A decrease up to 20% in the measured OCV, for $1°$ misalignment, for the highest measured frequency is recorded. Error introduced by lateral misalignments of up to $-5\,\mathrm{mm}$ and $5\,\mathrm{mm}$ both in Y and Z directions. A misalignment of $5\,\mathrm{mm}$ leads to a decrease in the measured OCV up to 60%, for the highest measured frequencies.

both the transmit sensitivity of the TX transducer and the receive sensitivity of the PMUT are considerably low in those ranges. Important to note is the low TX sensitivity of the transmitter also around the resonance frequency of PMUTs, which introduces an overall drop in the RX sensitivity of the measured devices, compared to the simulations. Additional 2D scans of the TX transducer have been carried out to evaluate the changes, not only in the intensity of the transmitted acoustic beam (**Fig. 5(e)**) but also in its profile, evaluated where the maximum intensity, in Z direction, was recorded. As illustrated in **Fig. 5(f)**, the higher the frequency, the narrower the acoustic beam gets. This, in turn, can influence the results obtained while measuring the OCV of the PMUTs. Assuming that misalignment can occur, if the beam, at high frequencies, is narrow or even narrower than the element under measurement (5x5 mm^2), a significant drop in the receive sensitivity can be observed. Additional factors, including measurement error, that can affect the results and cause discrepancies were explored in **Fig. 6**. To quantify the setup error, 10 consecutive measurements were performed on the same sample without changes, and the results indicated a maximum error of $\pm 2\%$ (**Fig. 6(a)**), around $5\,\mathrm{MHz}$, the resonance frequency of the TX transducer. The maximum error recorded for the resonance frequency of the PMUTs ($2.9\,\mathrm{MHz}$), however, is less than $\pm 0.5\%$, thus significantly low. Furthermore, setup changes introduce errors. Measurements on different days, requiring the sample to be removed from the stage or disassembling of the setup between measurements cause OCV fluctuations, even with the same settings (**Fig. 6(b)**). Equally important is the effect of misalignment. In **Fig. 6(c)**, both angular as well as lateral misalignment were evaluated. An angular misalignment, of even a $1°$ could potentially lead to a decrease of up to 20% in the measured OCV, for the highest measured frequency. For small lateral misalignments the effect does not appear to be as significant. However, it can be noted that a misalignment of $5\,\mathrm{mm}$ leads to a decrease in the measured

OCV of up to 60%, for the highest measured frequencies. Similar results have been previously simulated and reported in [27].

IV. CONCLUSION

This study evaluates the receive performance of polymer-coated PMUTs for implantable devices through simulations and experiments. All tested polymers exhibited high acoustic transparency (T>94%) at relevant thicknesses and frequencies, confirming their suitability for ultrasonic energy transfer. However, receive sensitivity is influenced not only by acoustic transmission but also by mechanical interactions between the coating and the PMUT membrane. Based on our results, three key material-related factors govern performance:

- Acoustic transparency, which ensures minimal signal attenuation through the coating;
- Acoustic impedance matching at interfaces, which reduces reflection losses;
- Flexural rigidity, which depends on both Young's modulus and thickness, and determines the extent to which the coating dampens membrane motion.

Stiffer coatings such as parylene-C reduced PMUT sensitivity but, when applied in thin layers, performed comparably to softer materials like MED2-4213, which preserved membrane mobility even at greater thicknesses. Similarly, TPU performed well, with good conformality. Finally, PCB substrate effects and setup variations were shown to impact measured sensitivity, underscoring the importance of system-level considerations. These findings offer a framework for designing effective PMUT encapsulation strategies.

REFERENCES

[1] L. Holzapfel and V. Giagka, "A robust backscatter modulation scheme for uninterrupted ultrasonic powering and back-communication of deep implants," *IEEE Transactions on Ultrasonics, Ferroelectrics, and Frequency Control*, vol. 71, pp. 1897–1905, 2024. DOI: `10.1109/TUFFC.2024.3465268`.

[2] L. Radziemski and I. R. S. Makin, "In vivo demonstration of ultrasound power delivery to charge implanted medical devices via acute and survival porcine studies," *Ultrasonics*, vol. 64, pp. 1–9, 2016. DOI: `10.1016/j.ultras.2015.07.012`.

[3] A. Rashidi, M. Saccher, C. B. Karuthedath, *et al.*, "An ultrasonically powered system using an AlN PMUT receiver for delivering instantaneous mW-range DC power to biomedical implants," in *IEEE International Ultrasonics Symposium (IUS)*, 2023. DOI: `10.1109/IUS51837.2023.10306557`.

[4] J. Charthad, M. J. Weber, T. C. Chang, and A. Arbabian, "A mm-sized implantable medical device (IMD) with ultrasonic power transfer and a hybrid bi-directional data link," *IEEE Journal of Solid State Circuits*, vol. 50, no. 8, pp. 1741–1753, 2015. DOI: `10.1109/JSSC.2015.2427336`.

[5] N. E. M. A. American Institute of Ultrasound in Medicine, *Standard for real-time display of thermal and mechanical indices on diagnostic ultrasound equipment*, Rockville, Md: The Institute. Print, 1992.

[6] A. Vanhoestenberghe and N. Donaldson, "Corrosion of silicon integrated circuits and lifetime predictions in implantable electronic devices," *Journal of Neural Engineering*, vol. 10, no. 3, 2013. DOI: `10.1088/1741-2560/10/3/031002`.

[7] K. Shen and M. M. Maharbiz, "Design of ceramic packages for ultrasonically coupled implantable medical devices," *IEEE Transactions on Biomedical Engineering*, vol. 67, no. 8, pp. 2230–2240, 2020. DOI: `10.1109/TBME.2019.2957732`.

[8] K. Nanbakhsh, A. S. Idil, C. Lamont, *et al.*, "On the longevity and inherent hermeticity of silicon-ICs: Evaluation of bare-die and PDMS-coated ICs after accelerated aging and implantation studies," *Nature Communications*, vol. 16, no. 12, 2025. DOI: `10.1038/s41467-024-55298-4`.

[9] K. Nanbakhsh, M. V. Gompel, R. Ritasalo, *et al.*, "An in vivo biostability evaluation of ALD and parylene-ALD multilayers as micro-packaging solutions for small single-chip implants," *Small*, 2025. DOI: `10.1002/smll.202410141`.

[10] D.-S. Lin, X. Zhuang, S. H. Wong, M. Kupnik, and B. T. Khuri-Yakub, "Encapsulation of capacitive micromachined ultrasonic transducers using viscoelastic polymer," *Journal of Microelectromechanical Systems*, vol. 19, no. 6, pp. 1341–1351, 2010. DOI: `10.1109/JMEMS.2010.2076786`.

[11] J. Oevermann, P. Weber, and S. H. Tretbar, "Encapsulation of capacitive micromachined ultrasonic transducers (CMUTs) for the acoustic communication between medical implants," *Sensors*, vol. 21, no. 2, 2021. DOI: `10.3390/s21020421`.

[12] S. Seok, "Polymer-based biocompatible packaging for implantable devices: Packaging method, materials, and reliability simulation," *Micromachines*, vol. 12, no. 9, 2021. DOI: `10.3390/mi12091020`.

[13] A. S. Idil, C. Lamont, K. Nanbakhsh, *et al.*, "On the stability of silicone-encapsulated CMOS ICs for active implantable devices: 4.3 years of accelerated life testing," *bioRxiv*, 2025. DOI: `10.1101/2025.05.21.655306`.

[14] A. I. Velea, J. Wilson, A. Gollhardt, C. B. Karuthedath, A. S. Thanniyil, and V. Giagka, "Non-monolithic fabrication of thin-film microelectrode arrays on PMUT transducers as a bimodal neuroscientific investigation tool," in *IEEE Engineering in Medicine and Biology (EMBC)*, 2023. DOI: `10.1109/EMBC40787.2023.10340770`.

[15] R. Hill and S. M. A. El-Dardiry, "Variables in the use and design of acoustic emission transducers," *Ultrasonics*, vol. 19, no. 1, pp. 9–16, 1981. DOI: `10.1016/0041-624X(81)90026-3`.

[16] R. Panskus, A. I. Velea, L. Holzapfel, *et al.*, "Ultrasound transparent neural interfaces for multimodal interaction," *BioRxiv*, Jul. 2025. DOI: `10.1101/2025.07.14.664713`.

[17] A. R. Selfridge, "Approximate material properties in isotropic materials," *IEEE Transactions on Sonics and Ultrasonics*, vol. 32, no. 3, pp. 381–394, 1985. DOI: `10.1109/T-SU.1985.31608`.

[18] A. I. Chen, M. L. Balter, M. I. Chen, *et al.*, "Multilayered tissue mimicking skin and vessel phantoms with tunable mechanical, optical, and acoustic properties," *Medical Physics*, vol. 43, no. 6, pp. 3117–3131, 2016. DOI: `10.1118/1.4951729`.

[19] P. Chen, A. M. A. O. Pollet, A. Panfilova, *et al.*, "Acoustic characterization of tissue-mimicking materials for ultrasound perfusion imaging research," *Ultrasound in Medicine Biology*, vol. 48, no. 1, pp. 124–142, 2022. DOI: `10.1016/j.ultrasmedbio.2021.09.004`.

[20] F. Levassort, L. P. Tran-Huu-Hue, P. Marechal, E. Ringgaard, and M. Lethiec, "Characterisation of thin layers of parylene at high frequency using PZT thick film resonators," *Journal of the European Ceramic Society*, vol. 25, pp. 2985–2989, 2005. DOI: `10.1016/j.jeurceramsoc.2005.03.208`.

[21] Z. Li, Z. Han, X. Jian, W. Shao, Y. Jiao, and Y. Cui, "Pulse-echo acoustic properties evaluation method using high-frequency transducer," *Measurement Science and Technology*, vol. 31, no. 12, 2020. DOI: `10.1088/1361-6501/aba0d8`.

[22] S. Imaoka, *Viscoelasticity (memo number: Sti0807a)*, `https://ansys-net.svsfem.cz/tips_sheldon/STI0807_Viscoelasticity.zip`, Ansys, Inc., Canonsburg, PA, 2008.

[23] Y. Kanbur and U. Tayfun, "Investigating mechanical, thermal, and flammability properties of thermoplastic polyurethane/carbon nanotube composites," *Journal of Thermoplastic Composite Materials*, vol. 31, no. 12, pp. 1661–1675, 2018. DOI: `10.1177/0892705717743292`.

[24] C. Hassler, T. Boretius, and T. Stieglitz, "Polymers for neural implants," *Polymer Physics*, vol. 49, no. 1, pp. 18–33, 2010. DOI: `10.1002/polb.22169`.

[25] B. J. Kim and E. Meng, "Micromachining of parylene c for biomems," *Polymers advanced technologies*, vol. 27, no. 5, pp. 564–576, 2016. DOI: `10.1002/pat.3729`.

[26] C. Chitrakar, E. Hedrik, L. Adegoke, and M. Ecker, "Flexible and stretchable bioelectronics," *Materials*, vol. 15, no. 5, 2022. DOI: `10.3390/ma15051664`.

[27] M. Saccher, A. Rashidi, A. S. Savoia, V. Giagka, and R. Dekker, "Phase distribution efficiency of cm-scale ultrasonically powered receivers," in *IEEE International Ultrasonics Symposium (IUS)*, 2023. DOI: `10.1109/IUS51837.2023.10307986`.

Andrada I. Velea (Graduate Student Member, IEEE) received her B.Sc. degree in electronics and telecommunications from the Polytechnic University of Timișoara, Romania, in 2017, and her M.Sc. degree (cum laude) in biomedical engineering from the Technical University of Delft, The Netherlands, in 2019, where she is currently pursuing her Ph.D., focusing on the investigation and development of active neural interfaces using ultrasound and electricity as means of neuromodulation. From 2020 to 2023, she was involved in the European project, Moore4Medical (M4M), which aimed to accelerate innovation in emerging medical applications through open technology platforms. Since 2020, she has also been a part of the Technologies for Bioelectronics Group, Fraunhofer Institute for Reliability and Microintegration IZM, Berlin, Germany.

Raphael Panskus received his B.Eng. degree in Microsystems Technology from the University of Applied Sciences (HTW), Berlin, Germany, in 2016, and the M.Sc. in Biomedical Engineering from the Berlin University of Technology, Berlin, Germany in 2020. He subsequently joined the Technologies for Bioelectronics Group at the Fraunhofer Institute for Reliability and Microintegration IZM, Berlin, Germany, as a Research Assistant. In 2021, he also became a member of the Bioelectronics Section at the Delft University of Technology, Delft, the Netherlands, where he is currently pursuing his Ph.D. focusing on the development of multimodal neural interfaces that integrate ultrasound technologies and electrophysiological techniques for imaging and neuromodulation.

Benedikt Szabo (Graduate Student Member, IEEE) is a PhD candidate at the Laboratory for Biomedical Microtechnology in the Department of Microsystems Engineering (IMTEK) and also part of the BrainLinks-BrainTools Center at the University of Freiburg. He studied Microsystems Engineering at the University of Freiburg and since 2020, he has been conducting research on neural electrodes and using ultrasound to power miniaturized neural implants.

Vera A. -L. Oppelt (Graduate Student Member, IEEE) is Head of Implantable Hardware Development at CorTec GmbH, a young medical device company focusing on the communication between the nervous system and innovative technology. She leads a cross-functional team of engineers working on peripheral interface development and implantable hardware integration. In addition to her management responsibilities, she is also a PhD candidate in the field of microsystems technology at the University of Freiburg, Germany, focusing on the functionality and reliability of implantable cuff electrodes. She holds a master's degree in medical microengineering and has presented her work at international conferences.

Lukas Holzapfel was born in Munich, Germany, in 1988. He received the M.Sc. in Electrical Engineering from the Technical University of Berlin, Berlin, Germany. As a student, he developed circuits for audio, industrial, and medical equipment at TIGRIS Elektronik GmbH, Berlin. Since 2020 he is working as a research assistant at Fraunhofer IZM, Berlin, Germany. He works on bioelectronic medicines, with a focus on power transfer and communication using ultrasound.

Cyril B. Karuthedath is a Senior Scientist at VTT Technical Research Centre of Finland., Espoo, Finland. He received his M.S. degree in Electrical Engineering from the Indian Institute of Technology Madras, Chennai, India, in 2013, and his Ph.D. degree in Electrical Engineering from Technische Universität München, Munich, Germany, in 2017. His areas of expertise include MEMS and sensor design and modeling, characterization, and interface circuit design. Since joining VTT in 2017, he has been actively involved in the development and system integration of Piezoelectric Micromachined Ultrasonic Transducers (PMUTs) and PMUT-based systems.

Abhilash T. Sebastian received his Ph.D. in physics from the University of Hyderabad, India, in 2010. Following his doctorate, he conducted postdoctoral research at the Tata Institute of Fundamental Research in India, Cornell University in the United States, and Aalto University in Finland. His research primarily focused on developing MEMS resonators using semiconductor nanowires, carbon nanotubes, and graphene to study nanoscale physics. Additionally, he worked on fabricating microfluidic devices for low-temperature applications. Since 2018, he has been a senior scientist at the VTT Technical Research Centre of Finland, specializing in the development of MEMS devices, particularly in the manufacturing of piezoelectric micromachined ultrasonic transducers (PMUTs).

Thomas Stieglitz (Fellow, IEEE) is full professor for Biomedical Microtechnology in the Department of Microsystems Engineering (IMTEK) and co-spokesperson of the BrainLinks-BrainTools Center at the University of Freiburg. He studied electrical engineering at the Universities of Braunschweig and Karlsruhe and received his PhD in 1998 from the University of Saarland (Saarbrücken, Germany). Dr. Stieglitz worked with the Frauhofer-Institute for Biomedical Engineering (St. Ingbert, Germany) from 1993 to 2004. Since 2004, he is with the University of Freiburg. His research interests include neural interfaces and implants and biocompatible assembling and packaging. He is co-founder of the neurotech start-ups CorTec and Neuroloop.

Alessandro S. Savoia (Member, IEEE) received the Laurea degree (M.S.) and the Ph.D. in Electronic Engineering from Roma Tre University, Italy, in 2003 and 2007, respectively. Since 2007, he has held a postdoctoral research position in the Department of Electronics Engineering at the same university. In the years 2008-2010 he participated, as a co-founder and R&D Manager, in an academic spin-off company of Roma Tre University, focused on the industrial exploitation of MEMS-based ultrasonic transducers (CMUTs). In 2014, he became Assistant Professor in Electronics at the Department of Engineering of Roma Tre University. In 2020, he obtained the National Scientific Qualification (ASN) for Full Professor in Electronics. His research interests are mainly focused on the development and system integration of MEMS ultrasonic transducers (CMUT and PMUT). Dr. Savoia serves the IEEE UFFC Society as Associate Editor for the IEEE Transactions on Ultrasonics, Ferroelectrics, and Frequency Control, and as Chair of the TPC Group 5 "Transducers and Transducer Materials" of the International Ultrasonics Symposium.

Vasiliki (Vasso) Giagka (Senior Member, IEEE) was born in Athens, Greece. She received the M.Eng. degree in electronic and computer engineering from the Aristotle University of Thessaloniki, Thessaloniki, Greece. She received the Ph.D. degree in Electronic Engineering from University College London, UK. She was a postdoctoral researcher at the Implanted Devices Group at University College London, UK. She is now an Associate Professor of Bioelectronics at Delft University of Technology (NL) and a research group leader at Fraunhofer Institute for Reliability and Microintegration IZM, Berlin (DE). Her research focuses on the fabrication of soft active multimodal neural interfaces. In particular, she investigates new approaches to reduce their size and increase their spatial resolution to meet the challenges of bioelectronic medicines.